Thermomechanical Characterization of Thermoplastic Polyimide–Polyurea to Improve the Chain Interaction via Internal Hydrogen Bonds

Alejandro Rivera Nicholls,[1] Matthew Pellisier,[1] Yesenia Perez,[1] John Allan Stock,[1] Ken Kull,[1] Tamalia Julien,[1] Jarrod Eubank ,[2] Julie P. Harmon [1]
[1]*University of South Florida, Tampa, Florida, 33620*
[2]*Florida Southern College, Lakeland, Florida, 33801*

Recently, we have studied polyimides (PIs) synthesized by incorporating an aromatic diamine monomer with a methylene linker, 4,4′-methylenebis(2,6-dimethylaniline), to make a robust main chain along with aliphatic polyetherdiamine backbone linkers to reduce rigidity. In this report, we incorporate a urea linkage into these materials in order to observe the effect of additional hydrogen bonding. The polymers are designed to exhibit thermal properties in between those of conventional aromatic PIs and polymers with wholly aliphatic ether diamine links. Herein, we demonstrate that the addition of 1,6 hexamethylene diisocyanate and the increase of hydrogen bonds at the urea linkage can be used to improve the thermal and mechanical properties of the PI. Furthermore, the imide ring is an important component to maintain the thermal stability characteristics in polyimide–polyurea hybrids. The polymers were characterized by FTIR, thermomechanical and calorimetric analysis, microhardness, and tensile testing. POLYM. ENG. SCI., 59:1948–1959, 2019. © 2019 Society of Plastics Engineers

INTRODUCTION

A series of thermoplastic polyimide–polyureas (PIUs) with tractable properties and structural improvements are synthesized and characterized in this work. Polyimides (PIs) with highly ordered aromatic backbones demonstrate high thermal stability, solvent resistance, low coefficients of thermal expansion, low dielectric constants, high glass transition temperatures, and superior mechanical properties [1–3]. These characteristics makes them a viable option in the production of high-performance products found in electronics, aerospace structural components, thermal insulation, composites, and adhesives [4–8]. Although PIs are relatively expensive compared with most polymer classes, the molecular architecture allows them to be tailored to produce an extensive combination of controllable properties. However, there are different synthetic methods [9–13] to manufacture this architectonical adaptable material. Hence, the chemistry of PIs is rather diverse with a variety of usable monomers and several methodologies available for synthesis.

The stability found in fully aromatic PIs renders them difficult to process due to highly elevated glass transition temperatures (T_gs) and the melt temperatures (T_ms), which range close to their decomposition temperatures [4–6, 14, 15]. The common process of manufacturing them involves preparing soluble polyamic acids, which are then coated as thin films on a surface to be later imidized by heat treatment to form the final PI; this technique leaves them exposed to hydrolysis or solvolysis before imidization occurs [16, 17]. The methodology also limits PIs to being cast as thin sheets with little postsynthetic processability for industrial applications. To circumvent these shortcomings, various groups have sought to break up the aromaticity of the PI backbone ultimately to impart thermoplastic behavior [7, 10, 17–22]by increasing flexibility and decreasing the different thermal transitions. The glass transition temperatures for a number of the resulting polymers remain relatively high, ranging from 215°C to over 310°C [7, 19–21]. Although these materials can be processed before decomposition, the temperature requirements remain elevated and reprocessing or recycling is unlikely. As the number of aliphatic linkers is increased, the flexibility of the backbone is improved, and therefore, the movement of the chains starts at a lower temperature. Baldwin et al. [23] used an entirely aliphatic ether as the diamine and reacted it with pyromellitic dianhydride (PMDA), reducing the glass transition temperature significantly (51°C to 75°C). These polymers lacked the highly ordered, stiff backbones of conventional PIs, and this loss of aromaticity greatly diminished the ability to compete with high-performance aromatic PIs. In our previous work [22], a series of PIs were designed to have tractable T_g using 4, 4′-methylenebis (2, 6-dimethylaniline) (MBDMA) with a wider range of glass transition temperatures (from 22°C to 101°C). Herein, we explore incorporating urea linkages into these PIs to enhance hydrogen bonding in an effort to further enhance thermal and mechanical properties [24].

Kull et al. [25] had previously investigated the behavior of polyurethanes and their interaction between the chains due to hydrogen bonding [26, 27]. The formation of polyurea characteristically implicates the quantifiable reaction between a diamine and a diisocyanate. This allows one to explore the merger of amine-terminated PI with isocyanate, creating a PI polyurea hybrid. The amalgamation could provide structural support by introducing hydrogen-bonding donors and acceptors in the backbone [26–28]. Polyureas represent a unique class of polymers that have found utility in a wide array of applications from protective coatings to foams and biomedical implants. The complement of hydrogen bonding provides advantageous solvent resistance garnering attention as thermally resilient thermoplastics. Polyureas have a lower decomposition temperature, around 200°C–330°C depending on their structural backbone [25, 29, 30]. Compared with PIs, the decomposition temperatures are lower [4–6, 22]. It is expected that the incorporation of the urea linkages into our PIs will have an influence on the thermal stability of the samples tested. The work done herein helps to merge two materials and improve their respective properties. The common usage of urea

Correspondence to: J. P. Harmon; e-mail: harmon@usf.edu
DOI 10.1002/pen.25196
Published online in Wiley Online Library (wileyonlinelibrary.com).

coatings[31, 32] and the high thermal resistance applications of PIs are combined in the proposed flexible PI enhanced by urea linkages. In the work shown by Feng and Iroh [31–33], the usage of a Kapton® -type PI precursor affords the high thermal stability but leads to processing issues. The PIU developed in this research leads to a flexible material that could be used in the corrosion resistance polymer coatings[31, 32]. In addition, lower thermal transitions provide larger processing windows. The thermal improvements can be seen as a large rubbery plateau due to crystallinity [25, 27], hydrogen bond reversible crosslinking [34], and high molecular weight [35]. The hydrogen bond could work as a reversible crosslinker and provides some self-healing properties [34]; this will be tested in future work. These thermal properties provide a large range of operational conditions for flexible materials. Single-use plastics have become an issue in today's economical and natural environment; it is important to consider the purpose of the material and the options after its life span. Polyureas can be recycled into carbamates to ensure they do not become a single-use plastic [36] on top of the multiple cycles the polymer could be used before it starts its recycling process.

In this work, PIUs are designed to serve as functional thermoplastic materials, which can be molded or extruded into shapes necessary for diverse uses, negating the need for the highly limiting thin-film polyamic acid casting methodology used with conventional PIs. In the case of these copolymers, the polypropylene-oxide diamine (PPODA; Jeffamine® D400) can interact with the isocyanate to create a urea bond and the dianhydride to form the imide ring. A modification to aliphatic PIs [22] in the interaction between the chains was used to enhance the thermal and mechanical properties. These are tuned by controlling the stoichiometric ratio of diisocyanate to the dianhydride per the introduction of H-bond donors from the urea linkages. The polymers are characterized by FTIR, thermomechanical and calorimetric analysis, tensile testing, and microhardness testing.

MATERIALS AND METHODS

Materials

3,3′,4,4'-Benzophenonetetracarboxylic dianhydride (BTDA), pyromellitic dianhydride (PMDA), 4,4′-methylenebis (2,6-dimethylaniline) (MBDMA), and gamma-butyrolactone (GBL) were used as received and donated from BrightVolt, Inc. (Lakeland, FL) [37, 38]. Jeffamine® D400 polypropylene-oxide diamine (PPODA) was donated by Huntsman, Inc. (The Woodlands, Texas). HPLC-grade tetrahydrofuran (THF) and 1,6-hexamethylene diisocyanate (HMDI) were used as received from Sigma Aldrich. Narrow molecular-weight polystyrene standards were purchased from Fluka Analytical.

Methods

General Procedure for Polymerization. PIs with different stoichiometric ratios of urea (Table 1), derived from HMDI, were synthesized (Fig. 1), creating approximately 250 g of PI in each reaction. First, a four-necked glass reactor was equipped with a mechanical mixer with Teflon blades, a nitrogen line, and a thermocouple. The reactor was placed inside a heating mantle and a distillation apparatus was assembled. The diamines (PPODA and MBDMA) were added to the reactor, which was sealed and kept at an inert nitrogen atmosphere for 24 h. Then, HMDI was added to the reactor to create a urea prepolymer. The mixture was homogenized with the mechanical mixer at 30°C for 20 min. Then, the dianhydride (BTDA or PMDA) was dissolved in GBL and added to the reactor. The temperature was increased to 80°C and the dianhydride (BTDA or PMDA) dissolved in GBL and added to the reactor was kept at that temperature under N_2 for 24 h. Water formed from the imidization of the polyamic acid ring was distilled using vacuum. The reaction yield was placed in a Teflon pan to oven cure at 200°C for 2 h to ensure complete closure of the imide ring. Then, it was further dried by storing it in a vacuum oven at 100°C. The different monomer fraction combinations are exemplified in Table 1.

Fourier Transform Infrared Spectroscopy/Attenuated Total Reflectance. Thin film samples were prepared in a heated Carver hydraulic press. The films were analyzed conducting 16 scans from 400 to 4,000 cm^{-1} at room temperature using a Spectrum One FT-IR (Perkin Elmer) equipped with ATR. The resulting data were collected in reflection mode and it was analyzed using the Spectrum software [39, 40].

Thermogravimetric Analysis. A 25 to 30 mg sample from each polymer formulation was assayed for temperature stability using a thermogravimetric analyzer TGA Q50 (TA Instruments) under nitrogen atmosphere. The samples were heated from 25°C to 600°C with a ramp rate of 10°C min^{-1}. The results were analyzed using the TA Universal Data Analysis software.

Characterization of Glass Transition Temperature by Differential Scanning Calorimetry and Dynamic Mechanical Analysis. Differential scanning calorimetry (DSC) analysis was carried out using a DSC 2920 differential scanning calorimeter (TA Instruments) over the temperature range from −30°C to 200°C. Temperature was calibrated using an indium standard. The samples were cut

TABLE 1. Stoichiometric formulations.

Sample	Modification of urea (%)	PMDA	BTDA	TMMDA	D400	HMDI
PI-1	0	0.50	N/A	0.10	0.40	0.00
PIU-1	10	0.40	N/A	0.10	0.40	0.10
PIU-2	20	0.30	N/A	0.10	0.40	0.20
PIU-3	30	0.20	N/A	0.10	0.40	0.30
PI-2	0	N/A	0.25	0.05	0.20	0.00
PIU-4	10	N/A	0.20	0.10	0.40	0.10
PIU-5	20	N/A	0.30	0.10	0.40	0.20
PIU-6	30	N/A	0.40	0.10	0.40	0.30

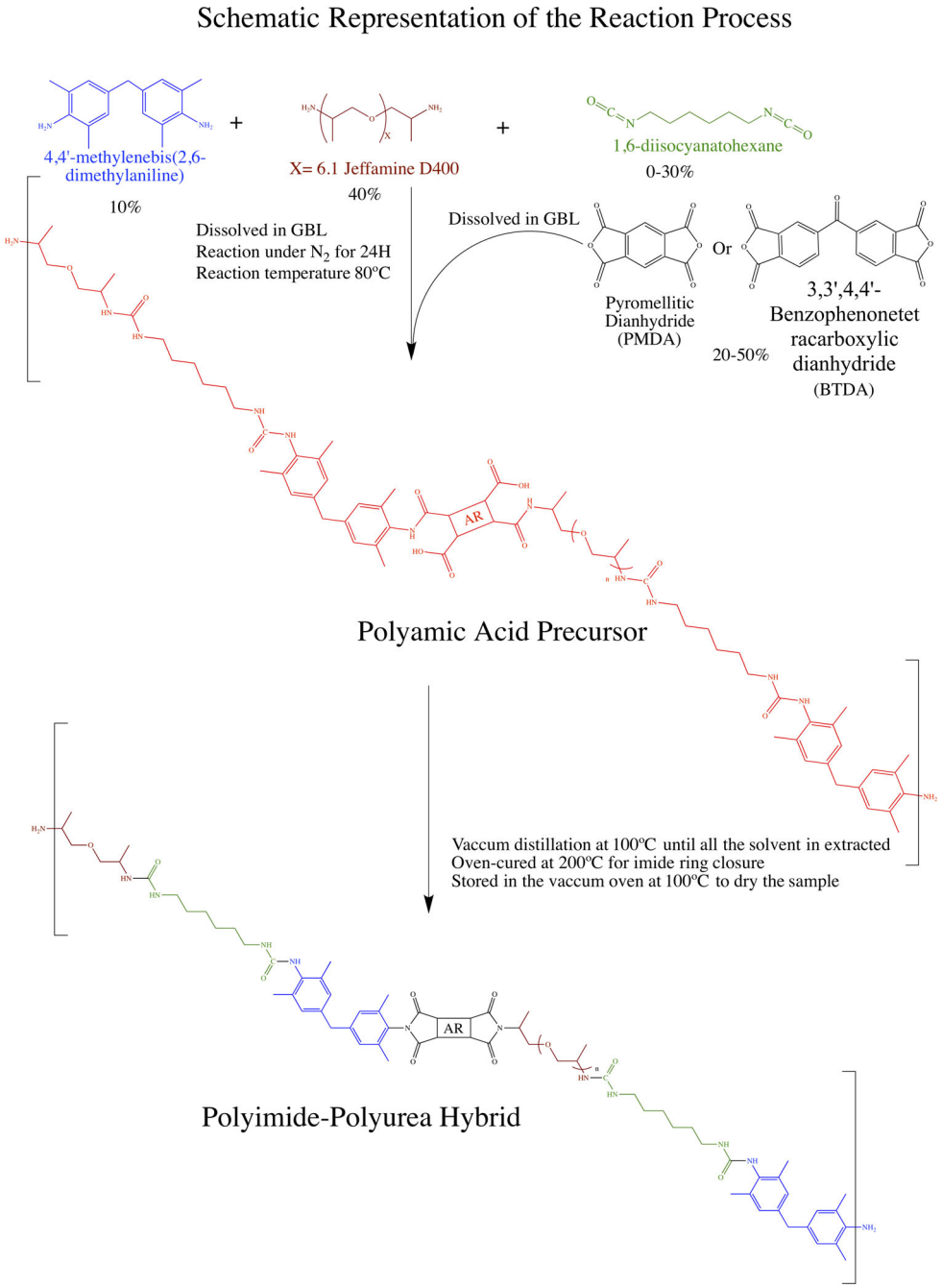

FIG. 1. Synthetic procedure for the formation of PIU copolymer. [Color figure can be viewed at wileyonlinelibrary.com]

and weighed; weights ranged from 9 to 10 mg. Samples were first heated from room temperature to 200°C at 20°C min^{-1}, cooled to −30°C at 20°C min^{-1}, and reheated to 200°C at 20°C min^{-1}. The cycle processes were used to erase thermal history due to sample preparation and storage. The results were analyzed using the TA universal analysis software and the second heating cycle was reported.

Dynamic mechanical analysis (DMA) was carried out on a rheometer AR2000 with a rectangular solid sample geometry. The samples (40 mm × 10 mm × 2 mm) were molded in a heated Carver hydraulic press at approximately 170°C with quick cooling to room temperature under 5 tons of pressure. Isothermal strain sweeps were performed on the rectangular samples to determine the linear viscoelastic regions (LVR) with an AR2000 rheometer (TA Instruments) at −50°C. The highest strain percent within the measured LVR was chosen to characterize the sample with a temperature ramp in the oscillation mode. Ramp conditions were −100°C to 300°C at 10°C min^{-1} and 1 Hz with liquid nitrogen used for cooling. The information was collected in an AR2000 rheometer by TA instruments using a TA Rheology Advantage software. Resulting data were analyzed with the TRIOS software available from TA Instruments.

Determination of Activation Energies of T_g via Dynamic Mechanical Analysis and Rheological Measurements. Rectangular bars of 40 mm in length, 10 mm in width, and 2 mm in thickness were molded in a Carver press. The samples were used to measure the activation energy of glass transition temperatures (T_gs). A time–temperature superposition (TTS) was made to calculate the activation energy using a William Landel Ferry (WLF) model. A range of frequencies from 0.05 to 10 Hz at constant temperatures below and above the T_g of the sample (−20°C to 150°C in 5°C increments) were used to obtain the information. Two common temperatures of 30°C and 50°C were used to generate the master curve of the samples to compare the activation energy. The information was collected in an AR2000 rheometer with a rectangular solid sample geometry by TA instruments using a TA Rheology Advantage software and analyzed using a TRIOS software.

Shore A Hardness Testing. Disks of 25 mm in diameter and 3 mm in thickness were molded in a Carver press. Measurements were made using the Shore Instrument & MFG. CO., INC Durometer type-A (ASTM D2240) hardness tester (New York). Six measurements were made on each specimen on both sides of the disk to check reproducibility. Averages and standard deviations were calculated from the six readings [41].

Tensile Testing. Films with a thickness between 0.1 and 0.2 mm were made using a Carver press. An ASTM D638 Type 5 die was used to cut the samples in the appropriate shape. Six dog-bone samples were cut out of each film and tested in the Shimadzu AGS-J. A 50 N force transducer (Model SM-50 N-168) was used to test the samples. Each dog-bone was pulled at 25 mm per min. The average for the six trials was reported in the results. The results were recorded and analyzed using the TrapeziumX Software.

RESULTS AND DISCUSSIONS

Infrared Spectroscopy

The Fourier transform IR spectra depicted the presence of the expected moieties in final products. This confirmed complete synthesis of the PIU hybrids [39, 40], which were formed through the imidization of a polyamic acid precursor. The infrared spectra of all synthesized PIU hybrids showed characteristic peaks of an imide moiety at around 1,771 and 1,714 cm^{-1}, which represent the stretching of the asymmetrical and symmetrical carbonyls located in the anhydride rings of the PMDA and BTDA monomer. Another characteristic peak of an imide moiety was observed at around 1,354 cm^{-1} for the C-N stretch from the aromatic carbon of the MBDMA monomer. Furthermore, another peak at around 730 cm^{-1} was seen for the carbonyl bending of the imide. The peak absences of the carboxylic acid and amide functional groups of the polyamic acid precursor showed that the imide ring was completely closed.

The final PIU products were expected to have a urea moiety, derived from the introduction of 1,6-disocyanohexane, which confirmed the presence of urea linkages. Absorption bands for the urea moiety were seen between 3,315 cm^{-1} and 3,374 cm^{-1}, representing the N—H stretch vibration of the amides from the isocyanate group (Fig. 2). The PIU hybrids synthesized with PMDA had stronger N—H-free stretch vibrations than the PIU hybrids with BTDA; however, the peak vibrations of all the PIU hybrids

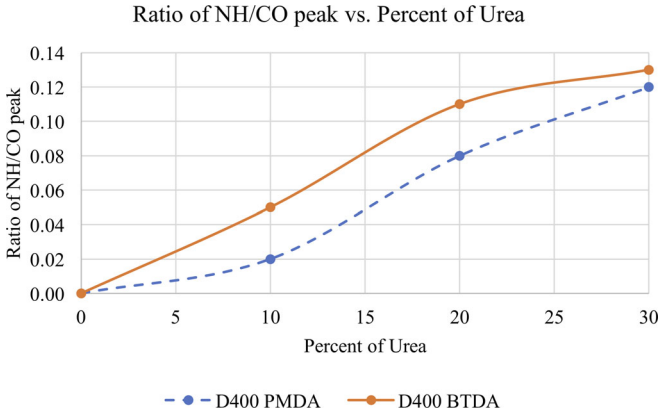

FIG. 2. Comparison between the PMDA and BTDA series for the incorporation of urea linkages with the increase of diisocyanate. [Color figure can be viewed at wileyonlinelibrary.com]

decreased as the stoichiometric ratio of urea was increased. Another characteristic peak that showed the presence of urea was around 1,642 cm^{-1} for the carbonyl stretch vibration of the PIU hybrids with PMDA and a peak around 1,670 cm^{-1} for the carbonyl stretch vibration of the PIU hybrids with BTDA. Other peaks observed in the PIU hybrids with PMDA were not the same as the peaks observed in the PIU hybrids with PMDA. The PIU hybrids with PMDA had N—H with C—N bending vibrations from the amide group in the backbone at around 1,546 cm^{-1}, C—N stretching vibrations at between 1,355 and 1,359 cm^{-1} from the part of the backbone derived from the dianhydride, C—O stretching vibrations at 1,300 cm^{-1}, C—O stretching vibrations near the imide moiety at 1,261–1,263 cm^{-1} from the PPODA, and C—O stretching vibrations around 1,092–1,095 cm^{-1} from the PPODA. However, in the PIU hybrids with BTDA, aromatic C═C stretching vibrations were seen at 1,483–1,427 cm^{-1} from BTDA, C—N stretching vibrations at 1367 cm^{-1} from the imide moiety, which was derived from the dianhydride monomer, C-N stretching vibrations at 1,294–1,247 cm^{-1}, and C—O stretching vibrations around 1,094 cm^{-1} from the PPODA monomer near isocyanate.

PI-1: ATR-IR (cm^{-1}): 1,771 cm^{-1} (asymmetric stretching C═O), 1,714 cm^{-1} (symmetric stretching C═O), 1,565 cm^{-1} (N—H mixed with C—N bending), 1,354 cm^{-1} (C—N stretching), 1,300 cm^{-1} (C—O stretching), 1,264 cm^{-1}(C—O stretching), 1,095 cm^{-1} (C—O stretching), and 730 cm^{-1} (C═O bending).

PIU-1: ATR-IR (cm^{-1}): 3,374 cm^{-1} (N—H free stretching), 1,771 cm^{-1} (asymmetric stretching C═O), 1,715 cm^{-1} (symmetric stretching C═O), 1,644 cm^{-1} (C═O stretching), 1,546 cm^{-1}(N—H mixed with C—N bending), 1,355 cm^{-1} (C—N stretching), 1,300 cm^{-1} (C—O stretching), 1,263 cm^{-1} (C—O stretching), 1,094 cm^{-1} (C—O stretching), and 730 cm^{-1} (C═O bending).

PIU-2: ATR-IR (cm^{-1}): 3,355 cm^{-1} (N—H free stretching), 1,771 cm^{-1} (asymmetric stretching C═O), 1,717 cm^{-1} (symmetric stretching C═O), 1,644 cm^{-1} (C═O stretching), 1,546 cm^{-1} (N-H mixed with C—N bending), 1,355 cm^{-1} (C—N stretching), 1,300 cm^{-1}(C—O stretching), 1,261 cm^{-1} (C—O stretching), 1,095 cm^{-1} (C—O stretching), and 730 cm^{-1} (C═O bending).

PIU-3: ATR-IR (cm^{-1}): 3,315 cm^{-1} (N—H free stretching), 1,772 cm^{-1} (asymmetric stretching C═O), 1,720 cm^{-1} (symmetric stretching C═O), 1,642 cm^{-1} (C═O stretching), 1,546 cm^{-1} (N—H mixed with C-N bending), 1,359 cm^{-1} (C—N stretching),

1,300 cm^{-1} (C—O stretching), 1,261 cm^{-1}(C—O stretching), 1,092 cm^{-1} (C—O stretching), and 730 cm^{-1} (C═O bending).

PI-2: ATR-IR (cm^{-1}): 1,772 cm^{-1} (asymmetric stretching C═O), 1,709 cm^{-1} (symmetric stretching C═O), 1,671 cm^{-1} (C═O stretching), 1,367 cm^{-1} (C—N stretching), 1,294 cm^{-1} (C—O stretching), 1,247 cm^{-1} (C—O stretching), 1,095 cm^{-1} (C—O stretching), and 728 cm^{-1} (C═O bending).

PIU-4: ATR-IR (cm^{-1}): 3,355 cm^{-1} (N—H free stretching), 1,773 cm^{-1} (asymmetric stretching C═O), 1,710 cm^{-1} (symmetric stretching C═O), 1,671 cm^{-1} (C═O stretching), 1,620 cm^{-1} (C═O stretching), 1,483–1,427 cm^{-1} (Ar—C═C stretching), 1,367 cm^{-1} (C—N stretching), 1,294–1,247 cm^{-1} (C—N stretching), 1,094 cm^{-1} (C—O stretching), and 727 cm^{-1} (C═O bending).

PIU-5: ATR-IR (cm^{-1}): 3,347 cm^{-1} (N—H free stretching), 1,773 cm^{-1} (asymmetric stretching C═O), 1,712 cm^{-1} (symmetric stretching C═O), 1,670 cm^{-1} (C═O stretching), 1,640 cm^{-1} (C═O stretching), 1,483–1,427 cm^{-1} (Ar—C═C stretching), 1,367 cm^{-1} (C—N stretching), 1,294–1,247 cm^{-1} (C—N stretching), 1,094 cm^{-1} (C—O stretching), and 727 cm^{-1} (C═O bending).

PIU-6: ATR-IR (cm^{-1}): 3,332 cm^{-1} (N—H free stretching), 1,774 cm^{-1} (asymmetric stretching C═O), 1,713 cm^{-1} (symmetric stretching C═O), 1,669 cm^{-1} (C═O stretching), 1,638 cm^{-1} (C═O stretching), 1,451 cm^{-1} (Ar—C═C stretching), 1,368 cm^{-1} (C—N stretching), 1,294–1,247 cm^{-1} (C—N stretching), 1,095 cm^{-1} (C—O stretching), and 727 cm^{-1} (C═O bending).

Thermogravimetric Analysis

The thermal stability and residual solvent retention of the PIU were evaluated by thermogravimetric analysis (TGA). The thermograms of the PIUs are shown in Fig. 3. The corresponding temperatures at 5% weight loss and the onset temperature are reported in Table 2. The diamine monomers and the lactone solvent used in processing both have boiling points around 205°C, which may explain the minimal loss of mass around that temperature. The stability at the onset temperature represents a relation between the different imide and urea bonds. Neat PIs typically have higher temperature stability [5, 6, 12] as their backbone is linear, well-ordered, rigid, and aromatic. The PIU synthesized in this article exhibit thermal onset stabilities that decrease as the glass transition temperatures decrease. The main variation in both series was the exchange from imide linkages to urea linkages. Aromatic PIs are recognized for having high thermal stability, but when the aromaticity is decreased with the incorporation of aliphatic monomers, the temperature stability decreases [22, 23]. On the other hand, polyureas have a lower temperature stability, especially if they are aliphatic [29–39, 42]. Therefore, the change from the imide ring to the urea link will have a tradeoff in temperature stability.

TABLE 2. Onset temperature and 5% loss.

Sample	Modification of urea (%)	Temperature at 5% loss (°C) (T_d)	Temperature at onset point (°C)
PI-2	Neat	356.42	355.25
PIU-4	10	320.92	302.70
PIU-5	20	279.51	271.96
PIU-6	30	293.36	301.83
PI-1	Neat	328.38	357.25
PIU-1	10	306.29	328.69
PIU-2	20	296.28	311.53
PIU-3	30	261.12	287.69

In the BTDA series, the data showed that the samples with a higher concentration of urea failed to attain the 300°C mark that was achieved by aliphatic PIs. The values ranged from 279°C to 356°C (Table 2). In the PMDA series, the trend continued when the temperature stability decreased as the polyurea started to increase and govern as the major bond in the polymer hybrid. The thermal stability varied between 261°C and 328°C (Table 2). The thermograms had a step in the 350°C to 370°C (Fig. 3) region and it occurred at a lower mass percentage as the concentration of urea in the polymer increased. The decomposition temperature (T_d) was above 260°C for each formulation verifying that the polymers were dry (Table 2). The information provided by TGA testing also allowed the determination of appropriate temperature ranges for DMA and DSC.

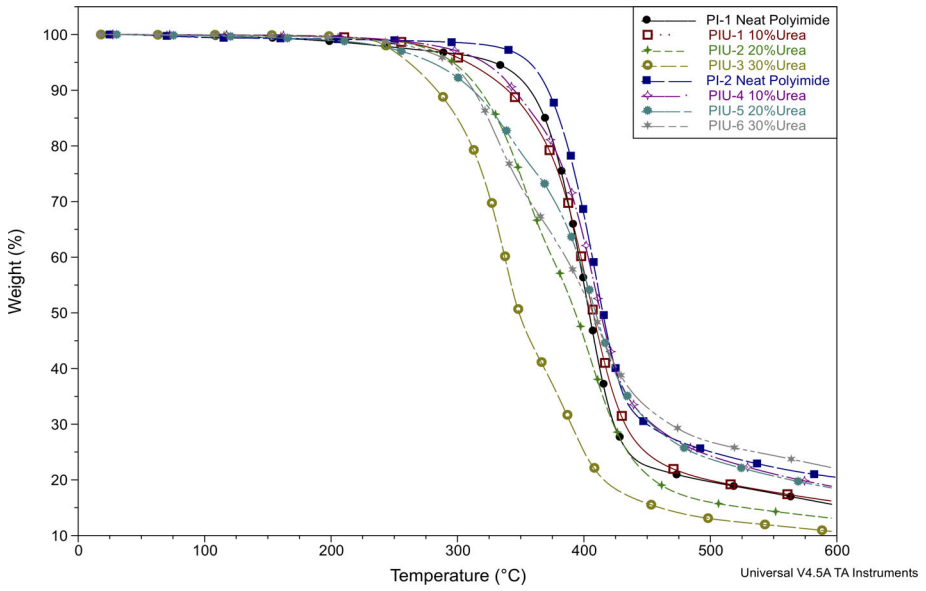

FIG. 3. Thermogram of PIU samples. [Color figure can be viewed at wileyonlinelibrary.com]

DOI 10.1002/pen

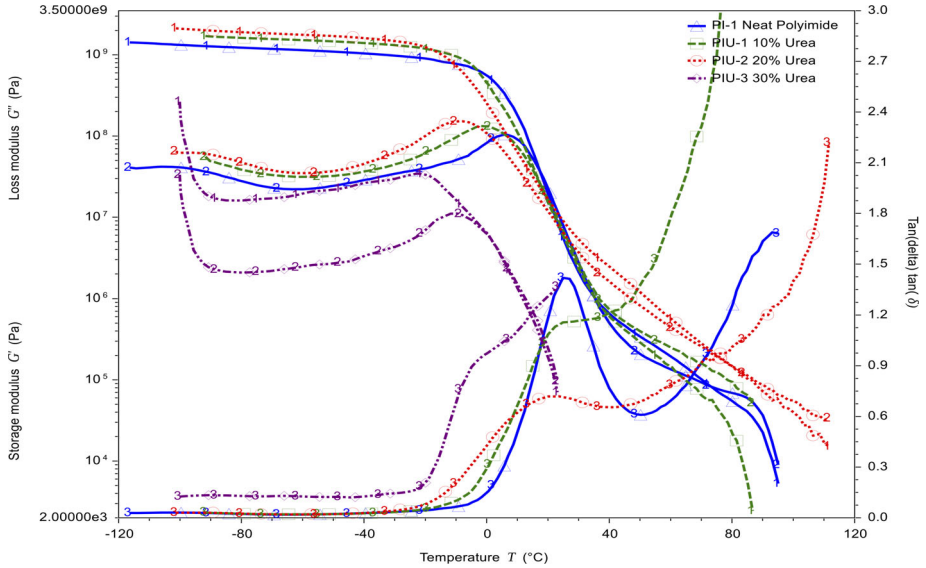

FIG. 4. Glass transition temperature of PMDA series (1 = *G*', 2 = *G*", and 3 = Tan Delta). [Color figure can be viewed at wileyonlinelibrary.com]

Characterization of Glass Transition Temperature (T_g) by Differential Scanning Calorimetry and Dynamic Mechanical Analysis

The glass transition temperature (T_g) was measured by two different techniques, DMA (Figs. 4 and 5), and DSC (Fig. 6). The different techniques allowed a detailed characterization of this important transition. The T_g in the DSC manifests as a step decrease in the heat capacity of the polymer and will be defined here as the mid-point of the curve between the original baseline heat capacity and the resulting heat capacity. In the DMA, the T_g was taken from the peak of the alpha transition from the loss modulus *G*" and the Tan δ [33]. At the three different temperatures, the polymer long-chain segmental motion is measured by a change in the baseline of the DSC, an increase in the loss modulus before a large drop, and finally an increase in the Tan δ close to the one in the ratio of the loss modulus over the storage modulus. In this set of series, the main variation is the addition of urea linkages in the backbone to study the contribution of hydrogen bonding in parallel to PIs having lower transition temperatures and still perform as robust PIs.

The T_g in these PIs is dominated by the urea linkage replacing the imide linkage to provide the hydrogen bond donors and acceptors to connect the chains in parallel. The T_g ranges from −10°C to 6°C from the loss modulus *G*" and from 0°C to 41°C from the loss factor Tan δ (Figs. 4 and 5), and from − 13°C to 34°C from DSC (Fig. 6 and Table 3). The imide ring provides a more robust rigid link than the aliphatic urea link. This can be appreciated in a

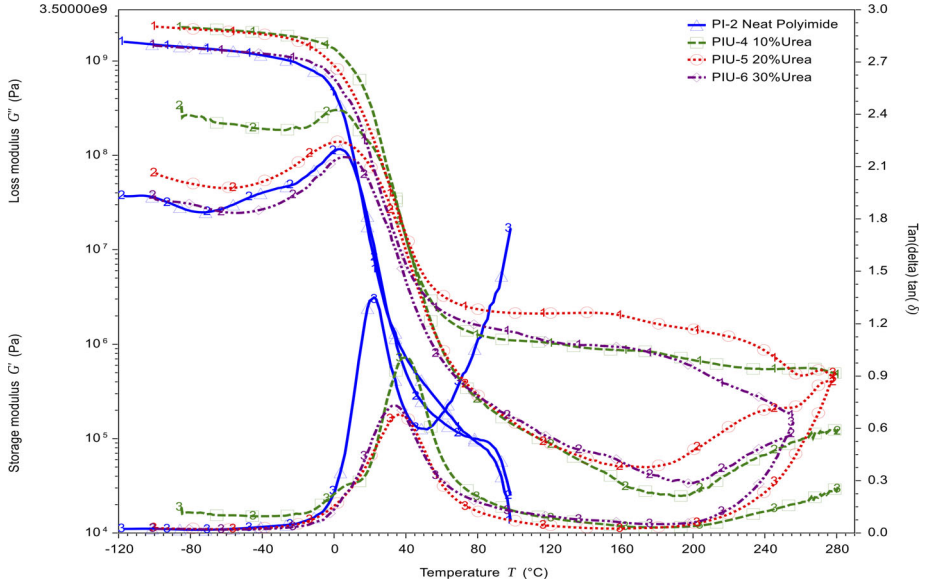

FIG. 5. Glass transition temperature of BTDA series (1 = *G*', 2 = *G*", and 3 = Tan Delta). [Color figure can be viewed at wileyonlinelibrary.com]

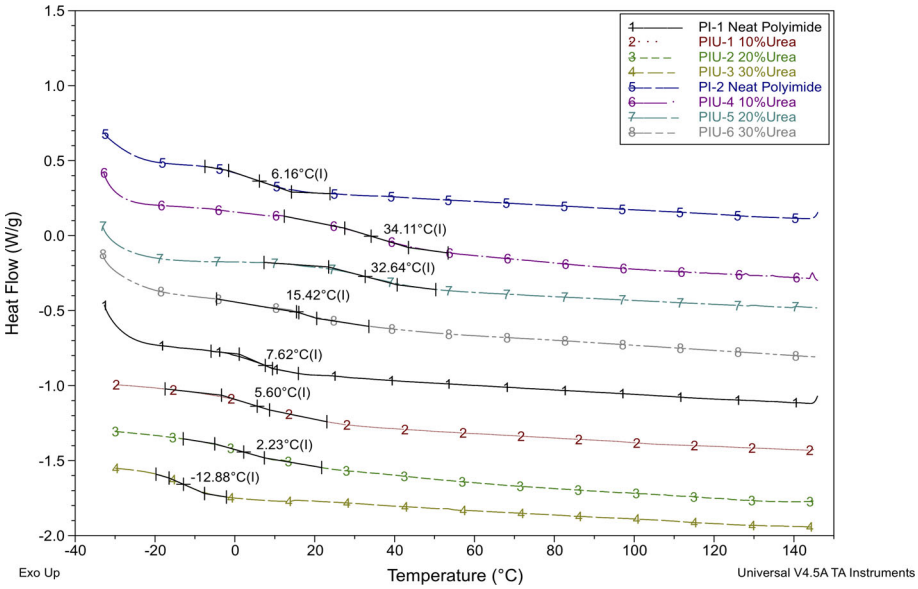

FIG. 6. Glass transition temperature of PMDA and BTDA series from DSC. [Color figure can be viewed at wileyonlinelibrary.com]

common pattern where it reaches a level of saturation where the governing link in the polymer is the urea over the imide. At this point, the flexible link with the help of the hydrogen bonding is not robust enough and the properties start to decline. Overall, the PI backbone can beneficiate from the presence of the urea linkages that provide some level of physical crosslinking [34] that improves the rubbery plateau. This is evidenced in Fig. 5 for the samples containing BTDA/D400 [27, 28]. The large rubbery plateau is of about 100°C (Fig. 5), and leads to the possibility of broader use applications. The storage modulus *G*' levels out after the T_g, forming a rubbery plateau at a higher value in the samples containing a urea linkage as than the neat sample (Fig. 5). In the PMDA/D400 series, the sample with 30% urea appeared softer, showing some blocking behavior; this was seen at room temperature when the samples fused with each other if they came in contact after molding. The low transition temperature allows for the chain slippage at room temperature. All the other samples kept their structures after molding them. The glass transition temperatures of the samples are low, but the large rubbery plateau in the BTDA samples (PIU-4, PIU-5, and PIU-6) shows that they can be used as robust polymers (Fig. 5). Owing to the presence of physical crosslinks, the behavior of the T_g is affected as well as the energy required to overcome that barrier.

Dynamic Mechanical Analysis and Rheological Analysis of Activation Energy for T_g

DMA was performed on rectangular solid samples under linear viscoelastic (LVE) strains determined from isothermal strain sweeps. Frequency sweeps at constant temperature under these LVE-determined strains yielded transitions as frequency-dependent increases of storage modulus *G*' and loss modulus *G*". Different temperatures, starting below the glass transition until the sample lost its structure, were used to determine a broad range of storage modulus *G*' and loss modulus *G*" at different temperatures and frequencies. The behavior of all the samples was common by having a large storage modulus *G*' close to 10^9 Pa when the temperature was below the T_g and the frequency was on the upper region of the measurement. At the end of the experiment, the moduli dropped 3 to 4 orders of magnitude close to 10^5 Pa (Figs. 4 and 5); this was achieved at low frequencies and higher temperatures.

The study of the activation energy of chain motion near the glass transition temperature was done using TTS (Figs. 7 and 9) and a WLF plot (Figs. 8 and 10). A common reference temperature in the viscoelastic region of the single frequency temperature ramp was selected (Table 4). The reference temperature is

TABLE 3. T_g characterization for PIU samples from DMA and DSC.

Sample	Modification of urea (%)	T_g from tan (δ) (°C)	T_g from *G*" (°C)	T_g from DSC (°C)	Storage modulus at −50°C
PI-1	Neat polyimide	24.88	5.74	7.62	1.09E + 09
PIU-1	10	22.34	−2.01	5.60	1.46E + 09
PIU-2	20	23.54	−7.97	2.23	1.70E + 09
PIU-3	30	0.46	−9.72	−12.88	2.20E + 07
PI-2	Neat polyimide	22.29	3.51	6.15	1.31E + 09
PIU-4	10	40.85	1.92	34.11	2.08E + 09
PIU-5	20	36.70	1.94	32.63	2.00E + 09
PIU-6	30	34.88	4.52	15.42	1.25E + 09

DOI 10.1002/pen

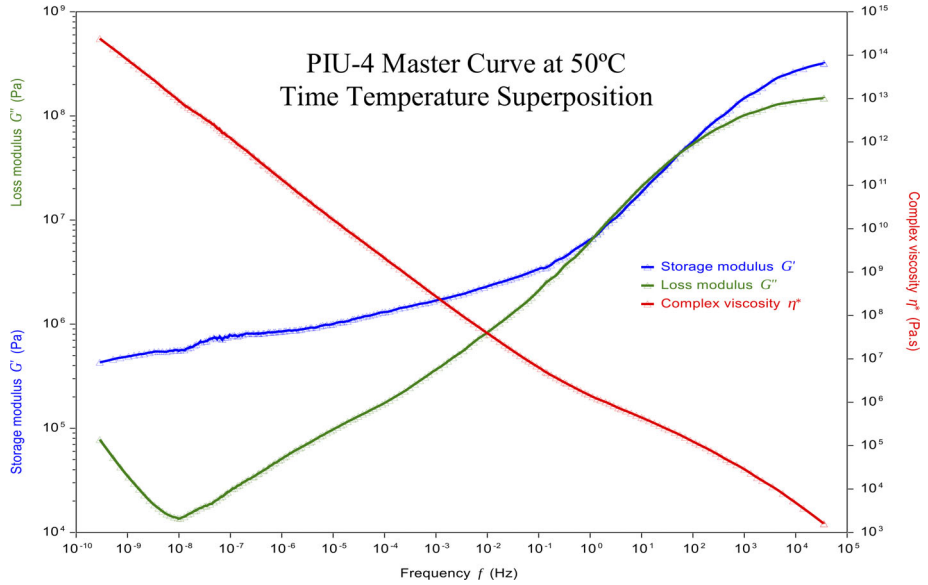

FIG. 7. TTS for the activation energy of the T_g of PIU-4. [Color figure can be viewed at wileyonlinelibrary.com]

typically situated between the glass transition temperature and T_g + 100°C, since this interval is valid to apply the WLF equation [43]. The temperatures were as follows: 30°C for the PMDA/D400 series and 50°C for the BTDA/D400 series (Figs. 7 and 9). The TTS plot allows the creation of a master curve for each polymer composition; this goes in combination with the WLF plot that plots the shift factor a_T with respect to temperature (Figs. 8 and 10) [43]. From the fitting of the curve using the WLF Eq. 1 is it possible to obtain the C_1 (B/2.303f_g) and C_2 (f_g/α_f) material constants, which are related to the free space (f_g) f and coefficient of thermal expansion (α_f) [35, 44]. In addition, Eq. 2 involves R for the universal gas constant, T for temperature, and T_g for the glass transition temperature [35, 44]; all these temperatures are in Kelvin.

$$Log(a_T) = \frac{-C_1(T-T_g)}{C_2+(T-T_g)} \quad (1)$$

$$\Delta E_a = 2.303\left(\frac{C_1}{C_2}\right)RT_g^2 \quad (2)$$

The activation energy of chain motion near the T_g region of most of the neat samples was lower than the samples that contained urea, which indicated that the introduction of H-bonds increased the activation energy by connecting the chains in series. The results presented in Table 4 showed that C_1 constants varied from 7.9 to 18.3, C_2 constants ranged from 76.7 to 172.7 K, and the activation energies from 136.8 to 214.9 kJ/mol (Table 4). The flexible diamine was a constant factor. PPODA provided the

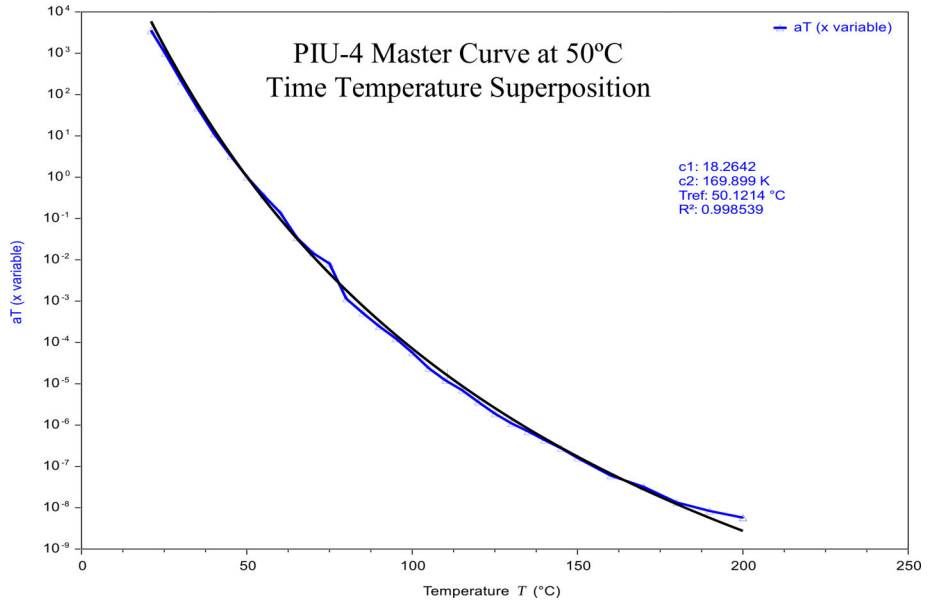

FIG. 8. WLF graph of PIU-4. [Color figure can be viewed at wileyonlinelibrary.com]

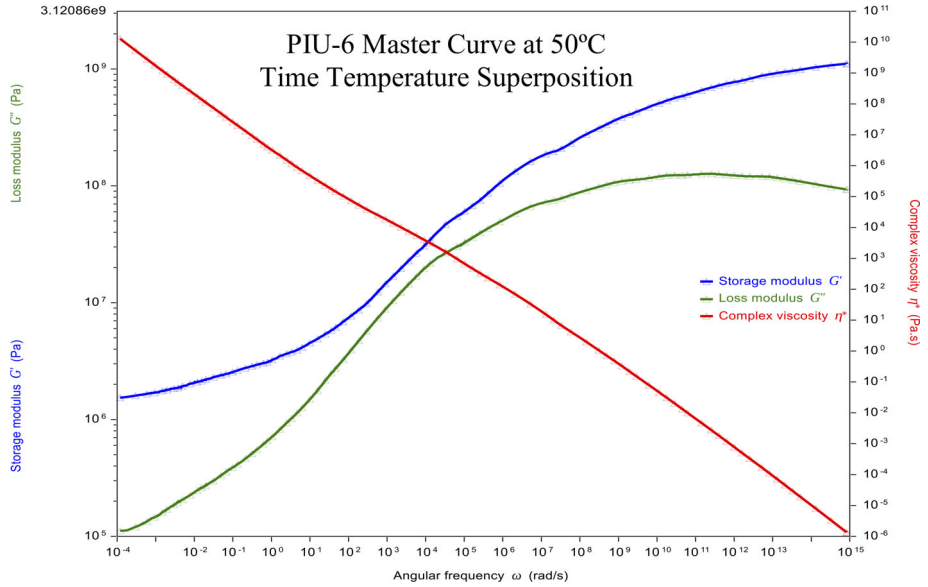

FIG. 9. TTS for the activation energy of the T_g of PIU-6. [Color figure can be viewed at wileyonlinelibrary.com]

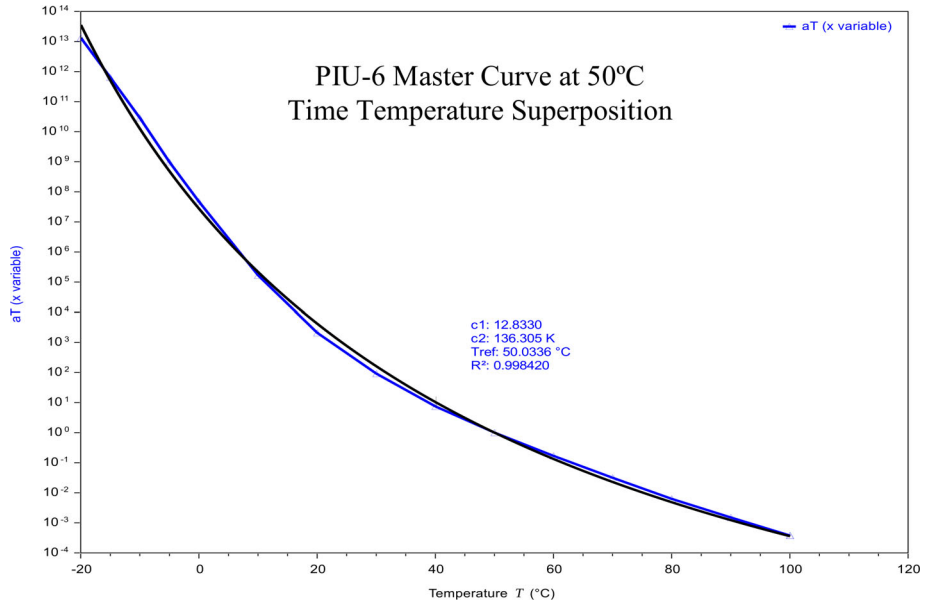

FIG. 10. WLF graph of PIU-6. [Color figure can be viewed at wileyonlinelibrary.com]

TABLE 4. Activation energy of T_g.

Sample	Modification of urea (%)	C1	C2(K)	Reference temperature (K)	R^2	Activation energy of T_g (kJ/Mol)
PI-1	Neat polyimide	7.85	76.75	303.15	0.9978	179.94
PIU-1	10	12.29	101.25	303.15	0.9989	213.60
PIU-2	20	10.36	96.76	303.15	0.9994	188.40
PIU-3	30	N/A	N/A	303.15	N/A	N/A
PI-2	Neat polyimide	14.30	141.28	323.15	0.9992	202.36
PIU-4	10	18.26	169.90	323.15	0.9985	214.94
PIU-5	20	11.82	172.70	323.15	0.9974	136.80
PIU-6	30	12.83	136.31	323.15	0.9984	188.25

 DOI 10.1002/pen

TABLE 5. Shore A hardness of the polyimide samples.

Series	Sample	Modification of urea (%)	Shore A
D400 PMDA	PI-1	Neat polyimide	10.8 ± 2.05
	PIU-1	10	24 ± 0.71
	PIU-2	20	41.6 ± 1.14
	PIU-3	30	N/A
D400 BTDA	PI-2	Neat polyimide	9.2 ± 0.45
	PIU-4	10	40.4 ± 2.70
	PIU-5	20	64.0 ± 1.41
	PIU-6	30	56.6 ± 2.51

flexibility in the backbone, and therefore, it had a low T_g and overall lower activation energy. An apparent difference in the dianhydrides was the extra aromatic ring in the BTDA compared with the PMDA, which increased T_g and the overall activation energies when keeping everything else the same. Since the T_gs were higher for the BTDA series, the reference temperature used was also higher, so even if the activation energy was in the similar range, a higher temperature was needed to reach the transition. The molecular weight of the sample can affect the T_g and, by consequence, the activation energy due to not reaching a critical entanglement point. The backbone contributed to a change in activation energy, but the main purpose was the impact of the urea linkages added to the polymer and the hydrogen bonds they provided between the chains. This physical crosslinking effect connects the chains in parallel to help minimize the effect of molecular weight. The activation energy is related to the T_g. With a high glass transition temperature, the activation energy needed to promote the slippage of the main chains needs to be greater. The two types of links that govern the samples show a similar behavior. The robust imide ring and the aliphatic urea link provided different types of restrictions in the movement of the chains that affect the activation energy. It shows that the 10%urea sample in both series have the most constructive interference achieving the higher activation energy for both samples. After that it decreases in the 20%urea sample due to the exchange of the imide rigidity to the urea plasticity. Finally, only the 30%urea sample from the BTDA was stable to be tested and shows a rise in activation energy due to the decrease in the chained mobility caused by the increased hydrogen bond sites. The overall patterns of the samples are shown below:

- PI-1 (0%) < PIU-2 (20%) < PIU-1 (10%) [PPODA and PMDA] (Table 4)
- PIU-5 (20%) < PIU-6 (30%) < PI-2 (0%) < PIU-4 (10%) [PPODA and BTDA] (Table 4)

The activation energy is related to multiple factors that interfere with the movement of the chains and prevent their slippage. The different elements show a constructive interference in the behavior of the activation energy of chain motion near the T_g region.

Shore A Hardness Test

Disks of 25 mm were indented multiple times on both sides of the sample to account for sample anisotropy differences during the preparation. A Shore A indenter was used to dent the samples and obtain the Shore A hardness [41]. The results of the indentations are presented in Table 5. Overall the hardness is determined by the backbone and the interaction of the polymer chains. The main variation of diisocyanate to replace the dianhydride and include some hydrogen bonding showed a similar trend. Furthermore, it shows the presence of the H-bonding groups in the aliphatic component and how they affect the hardness of the PIs. The common behavior of the samples shows that as the H-bonding is increased, the hardness increases up to the point where the main links of the polymer change from imide to urea. The samples had a Shore A value ranging from 11 to 42 for PMDA and 9 to 64 for BTDA (Table 5). Only the sample of PMDA with 30% diisocyanate in the composition did not make a sample that was possible to be tested and it shows blocking behavior by adhering to itself, which prevented the manufacture of a disk. The H-bonding introduced by the urea linkages increased the interaction in parallel between the chains, which is also connected to the T_g and has the same behavior. The higher interaction between the chains increased the hardness and the T_g, but the main behavior was governed by the imide linkage over the urea linkage. The imide ring provided the stability, while the aliphatic urea linkage provided the H-bonding as compliment.

Tensile Testing

The effect of urea linkages on force per area (stress) and elongation (strain) values was observed for the PIs formulations containing a PPODA. When PPODA was combined with a dianhydride, BTDA or PMDA, it made a flexible polymer [22]; the introduction of the H-bond donors from the urea increased the interaction between the chains and affected the tensile properties [26–28]. The results from the inclusion of the urea component can be seen in Table 6. The properties of the polymer are improved, providing that the main linkage is the imide ring;

TABLE 6. Tensile testing results for PIU samples.

Sample	Urea (%)	Stress at Break (N/mm^2)	Strain at Break (%)	Stress at Max (N/mm^2)	Strain (%) at Max	Young's Modulus (N/mm^2)	Yield point stress (N/mm^2)	Yield point strain (N/mm^2)
PI-1	0	0.87 ± 0.05	1,058 ± 71.9	1.04 ± 0.11	641.6 ± 19.3	0.0098 ± 0.001	0.621 ± 0.06	127 ± 57.2
PIU-1	10	1.30 ± 0.20	617.4 ± 87.5	1.40 ± 0.20	587.5 ± 106	0.024 ± 0.008	0.627 ± 0.08	51.3 ± 12.3
PIU-2	20	3.21 ± 0.16	340.2 ± 25.3	3.39 ± 0.16	318.7 ± 32.1	0.15 ± 0.02	2.01 ± 0.05	35.0 ± 5.60
PIU-3	30	N/A	N/A	N/A	N/A	N/A	N/A	N/A
PI-2	0	9.89 ± 0.72	176.4 ± 36.6	11.26 ± 0.48	157.5 ± 24.2	2.82 ± 0.45	9.04 ± 0.79	7.90 ± 2.54
PIU-4	10	11.7 ± 2.38	292.9 ± 35.7	11.56 ± 1.76	267.0 ± 30.3	0.22 ± 0.07	2.44 ± 0.50	24.19 ± 3.22
PIU-5	20	16.3 ± 2.23	444.2 ± 84.6	16.97 ± 1.81	438.8 ± 77.3	0.11 ± 0.02	2.67 ± 0.34	47.0 ± 9.74
PIU-6	30	8.28 ± 0.44	79.42 ± 19.1	8.44 ± 0.41	77.50 ± 18.7	0.42 ± 0.16	4.11 ± 0.39	16.0 ± 3.41

once the concentration of urea linkage dominates, the stress and strain start to decrease. The rigid imide ring has a more robust structure than the urea linkages, even though it is helped by the H-bonding.

The behavior in both series is related to the dominance of the major linkage but differ in the strain trend. In the BTDA series, first, the stress values ranged from 8.3 to 16.4 N/mm^2 at break and 8.4 to 17.0 N/mm^2 at max. Second, the strain values ranged from 79.4% to 444.2% at break and 77.5% to 438.8% at max (Table 6). In both the cases, the uppermost stress and strain was achieved for the sample containing 20% urea and the bottommost value for the sample containing 30% urea. The properties of the 10% urea sample were improved when compared with the neat BTDA PI and fall in the middle of the series range. The only considerable change in behavior comes from the decrease of yield strength for the urea samples compared with the BTDA neat PI; otherwise, the addition of the H-bond increases the ultimate tensile strength. In the PMDA series, first, the stress values ranged from 0.9 to 3.2 N/mm^2 at break and 1.0 to 3.4 N/mm^2 at max. Moreover, the strain values ranged from 340.2% to 1,057.7% at break and 318.7% to 641.6% at max (Table 6). The 30%urea sample in this series did not create a proper film that could be tested. In the results of the stress, the highest value was achieved for the sample containing 20% urea and the lowest value for the PMDA neat PI sample. In the outcomes of the strain, the highest value was achieved for the neat sample and the lowest value for the sample containing 20% urea.

The results of the tensile testing support the indication that the physical properties of the polymer can be improved with the addition of the urea linkages if it remains in the PI domain. Compared with aromatic PIs like Kapton (DuPont) and Ultem (G.E), the stress is only a fraction of what they can achieve, but the strain is highly improved, and it is all due to the aliphatic PPODA and the HMDI.

CONCLUSIONS

Fully aromatic PIs are well known to exhibit high thermal stability and resistance to solvents, due to the interaction between the aromatic rings and the closed packing of the chains. On the other hand, PIs with aliphatic diamines have fewer interactions between the chains, which lowers the thermal and physical stabilities that aromatic PIs are known to exhibit. The incorporation of the aliphatic diisocyanate introduces a urea linkage into the backbone. This increases the flexibility of the polymer, but at the same time, it upsurges the interaction in parallel between the polymer chains. The processability of aliphatic PIs compared with fully aromatic PIs is improved, and the thermal and physical stabilities compared wit the aliphatic PIs are enhanced. This work provides an expansion in applications for aliphatic PIs and a merger with polyureas. By maintaining long-chain aliphatic polyetherdiamines, one could impart flexible components into the backbone, making our PIU melt processable. This allows using thermoplastic techniques such as compression molding, injection molding, and extrusion. Thermal and mechanical properties, such as decomposition temperatures and microhardness, revealed a wider range of processability and lead to the elimination or reduction of the solvent used for the separator layer/electrolyte composites. All of this will lead to lower energy expenses. Rheological analysis (1 Hz) showed glass transition temperatures (T_g), ranging from approximately 0.5°C to 40.8°C, and an increase in the rubbery plateau in the BTDA due to the improvement provided by hydrogen bonding. The flexible component came from the diamine portion of the PI, but the modifications at the dianhydride side with the aliphatic diisocyanate introduced a second plastic component.

ACKNOWLEDGMENTS

This research was supported through the generous donations of Jeffamine® D-Series diamines from Huntsman International LLC© and of solvents, monomers, and various consumables from Brightvolt©.

REFERENCES

1. W. Qu, T.-M. Ko, R.H. Vora, and T.-S. Chung, *Polymer*, **42**(**15**), 6393 (2001).
2. Y. Han, X.Z. Fang, and X.X. Zuo, *Express Polym. Lett.*, **4**(**11**), 712 (2010).
3. R. Hariharan, S. Bhuvana, M.A. Malbi, and M. Sarojadevi, *J. Appl. Polym. Sci.*, **93**(**4**), 1846 (2004).
4. N. Regnier and C. Guibe, *Polym. Degrad. Stab.*, **55**(**2**), 165 (1997).
5. L. Li, C. Guan, A. Zhang, D. Chen, and Z. Qing, *Polym. Degrad. Stab.*, **84**(**3**), 369 (2004).
6. A.C. Lua and J. Su, *Polym. Degrad. Stab.*, **91**(**1**), 144 (2006).
7. Yang H, Liu J, Ji M, Yang S. Novel Thermoplastic Polyimide Composite Materials: INTECH Open Access Publisher, 2012
8. M. Ghosh, *Polyimides: Fundamentals and Applications*, CRC Press, New York (1996).
9. S. Xia, Z. Sun, L. Yi, and Y. Wang, *RSC Adv.*, **3**(**34**), 14661 (2013).
10. Y. Han, X.-Z. Fang, and X.-X. Zuo, *High Perform. Polym.*, **22** (**8**), 989 (2010).
11. T. Namikoshi, K. Odahara, A. Wakino, M. Murata, and S. Watanabe, *High Perform. Polym.*, **27**(**2**), 183 (2014). https://doi.org/10.1177/0954008314542474.
12. T. Inoue, Y. Kumagai, M.-A. Kakimoto, Y. Imai, and J. Watanabe, *Macromolecules*, **30**(**7**), 1921 (1997).
13. Y. Kumagai, K. Itoya, M.A. Kakimoto, and Y. Imai, *J. Polym. Sci. A Polym. Chem.*, **38**(**8**), 1391 (2000).
14. X. Pei, G. Chen, Y. Hou, and X. Fang, *High Perform. Polym.*, **25** (**3**), 312 (2013).
15. M.A. Takassi, A. Zadehnazari, A. Farhadi, and S. Mallakpour, *Prog. Org. Coat.*, **80**, 142 (2015).
16. K. Noda, C. Hiroki, S. Dai, and S. Kazuya, Method of producing polyimide resin, method of producing polyimide coating, method of producing polyamic acid solution, polyimide coating, and polyamic acid solution. U.S. Patent 9,458,355, filed 20 August 2013 and issued 4 October 2016 (2013).
17. S. Takabayashi and M. Tooru, Method for producing polyimide film and polyamic acid solution composition. U.S. Patent 8,906,463, issued December 9, 2014 (2014).
18. K.B. Shepard, H. Gevgilili, M. Ocampo, J. Li, F.T. Fisher, and D.M. Kalyon, *J. Polym. Sci. B Polym. Phys.*, **50**(**21**), 1504 (2012).
19. A. Kumar, S. Tateyama, K. Yasaki, M.A. Ali, N. Takaya, R. Singh, and T. Kaneko, *Polymer*, **83**, 182 (2016).
20. Y. Han, X.Z. Fang, and X.X. Zuo, *J. Mater. Sci.*, **45**(**7**), 1921 (2010).

21. S.-H. Hsiao, Y.-H. Hsiao, and Y.-R. Kung, *J. Electroanal. Chem.*, **764**, 31 (2016).
22. A. Rivera Nicholls, K. Kull, C. Cerrato, et al., *Polym. Eng. Sci.*, **59**(**2**), 221 (2019). https://doi.org/10.1002/pen.24893.
23. A.F. Baldwin, R. Ma, C. Wang, R. Ramprasad, and G. A. Sotzing, *J. Appl. Polym. Sci.*, **130**(**2**), 1276 (2013).
24. B.J. Folmer, R. Sijbesma, R. Versteegen, J. Van der Rijt, and E. Meijer, *Adv. Mater.*, **12**(**12**), 874 (2000).
25. K.L. Kull, R.W. Bass, G. Craft, T. Julien, E. Marangon, C. Marrouat, and J.P. Harmon, *Eur. Polym. J.*, **71**, 510 (2015).
26. L. Ning, W. De-Ning, and Y.J.M. Sheng-Kang, *Macromolecules*, **30**(**15**), 4405 (1997).
27. S. Sami, E. Yildirim, M. Yurtsever, E. Yurtsever, E. Yilgor, I. Yilgor, and G.L. Wilkes, *Polymer*, **55**(**18**), 4563 (2014). https://doi.org/10.1016/j.polymer.2014.07.028.
28. Das S, Cox DF, Wilkes GL, et al. *J. Macromol. Sci. B*, 2007; **46** (**5**):853–75 doi: https://doi.org/10.1080/00222340701388805.
29. J.-C. Zhao, F.-P. Du, X.-P. Zhou, et al., *Compos. Part B Eng.*, **42** (**8**), 2111 (2011). https://doi.org/10.1016/j.compositesb.2011.05.005.
30. J.M. Dennis, L.I. Steinberg, A.M. Pekkanen, J. Maiz, M. Hegde, A.J. Müller, and T.E. Long, *Green Chem.*, **20**(**1**), 243 (2018). https://doi.org/10.1039/c7gc02996a.
31. L. Feng and J.O. Iroh, *Prog. Org. Coat.*, **77**(**3**), 590 (2014). https://doi.org/10.1016/j.porgcoat.2013.11.023.
32. L. Feng and J.O. Iroh, *J. Appl. Polym. Sci.*, **135**(**9**) (2018). https://doi.org/10.1002/app.45861.
33. L. Feng and J.O. Iroh, *Eur. Polym. J.*, **49**(**7**), 1811 (2013). https://doi.org/10.1016/j.eurpolymj.2013.04.007.
34. R. Martin, A. Rekondo, A. Ruiz de Luzuriaga, G. Cabañero, H. J. Grande, and I. Odriozola, *J. Mater. Chem. A*, **2**(**16**), 5710 (2014). https://doi.org/10.1039/c3ta14927g.
35. M.T. Shaw and W.J. MacKnight, *Introduction to Polymer Viscoelasticity*. 4th ed., John Wiley & Sons, Hoboken (2018).
36. Q. Li, P. Wang, S. Liu, Y. Fei, and Y. Deng, *Green Chem.*, **18** (**22**), 6091 (2016). https://doi.org/10.1039/c6gc01884j.
37. C.G. Wensley, A. Vallée, D. Brouillette, and S. Gustafson, Google Patents (2007).
38. C.G. Wensley, S. Gustafson, C.R. Nelson, R.W. Singleton, A. Vallee, and D. Brouillette, Avestor LP and Solicore Inc. Polyimide matrix electrolyte and improved batteries therefrom. U.S. Patent 7,129,005, filed 27 April 2005 and issued 31 October 2006 (2006).
39. H. Zhang and X. Wang, *Sol. Energy Mater. Sol. Cells*, **93**(**8**), 1366 (2009). https://doi.org/10.1016/j.solmat.2009.02.021.
40. J. Li, X. Yuan, S. Liu, Z. He, Z. Zhou, and L.A.A. Low-Cost, *ACS Appl. Mater. Interfaces*, **9**(**38**), 32643 (2017). https://doi.org/10.1021/acsami.7b07437.
41. A. Siddiqui, M. Braden, M.P. Patel, and S. Parker, *Dent. Mater.*, **26**(**6**), 560 (2010). https://doi.org/10.1016/j.dental.2010.02.004.
42. L. Yuan, G.-Z. Liang, J.-Q. Xie, J. Guo, and L. Li, *Polym. Degrad. Stab.*, **91**(**10**), 2300 (2006). https://doi.org/10.1016/j.polymdegradstab.2006.04.026.
43. M.L. Williams, R.F. Landel, and J.D. Ferry, *J. Am. Chem. Soc.*, **77**(**14**), 3701 (1955).
44. J.J. Aklonis and W.J. Macknight, *Introduction to Polymer Viscoelasticity*, American Chemical Society, Washington, DC (1984).